

RESEARCH ARTICLE | OCTOBER 23 2024

Quantum enhanced mechanical rotation sensing using wavefront photonic gears

Special Collection: [Angular Momentum of Light](#)

Ofir Yesharim ; Guy Tshuva ; Ady Arie  



APL Photonics 9, 106116 (2024)

<https://doi.org/10.1063/5.0231506>



Articles You May Be Interested In

Witnessing entangled two-photon absorption via quantum interferometry

APL Photonics (March 2023)

Scalable multiphoton quantum metrology with neither pre- nor post-selected measurements

Appl. Phys. Rev. (October 2021)

Generating and breeding optical Schrödinger's cat states

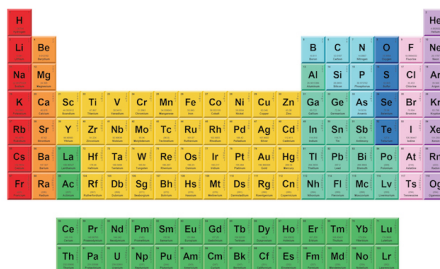
AIP Conference Proceedings (February 2018)

08 November 2024 17:29:35



THE MATERIALS SCIENCE MANUFACTURER®

Now Invent.™



American Elements
Opens a World of Possibilities

...Now Invent!

www.americanelements.com

© 2021-2024 American Elements is a U.S. Registered Trademark

Quantum enhanced mechanical rotation sensing using wavefront photonic gears

Cite as: APL Photon. 9, 106116 (2024); doi: 10.1063/5.0231506

Submitted: 31 July 2024 • Accepted: 11 October 2024 •

Published Online: 23 October 2024



View Online



Export Citation



CrossMark

Ofir Yesharim,  Guy Tshuva,  and Ady Arie^{a)} 

AFFILIATIONS

School of Electrical Engineering, Iby and Aladar Fleischman Faculty of Engineering, Tel Aviv University, Ramat Aviv, 69978 Tel Aviv, Israel

Note: This paper is part of the Special Topic on Angular Momentum of Light.

^{a)}**Author to whom correspondence should be addressed:** ady@tauex.tau.ac.il

ABSTRACT

Quantum metrology leverages quantum correlations for enhanced parameter estimation. Recently, structured light enabled increased resolution and sensitivity in quantum metrology systems. However, lossy and complex setups impacting photon flux hinder true quantum advantage while using high dimensional structured light. We introduce a straightforward mechanical rotation quantum sensing mechanism, employing high-dimensional structured light and use it with a high-flux (45 000 coincidence counts per second) N00N state source with $N = 2$. The system utilizes two opposite spiral phase plates with topological charge of up to $\ell = 16$ that converts mechanical rotation into wavefront phase shifts and exhibit a 16-fold enhanced super-resolution and 25-fold enhanced sensitivity between different topological charges, while retaining the acquisition times, and with negligible change in coincidence count. Furthermore, the high efficiency together with the high photon flux enables detection of mechanical angular acceleration in real-time. Our approach paves the way for highly sensitive quantum measurements, applicable to various interferometric schemes.

© 2024 Author(s). All article content, except where otherwise noted, is licensed under a Creative Commons Attribution (CC BY) license (<https://creativecommons.org/licenses/by/4.0/>). <https://doi.org/10.1063/5.0231506>

I. INTRODUCTION

Quantum metrology is a promising avenue in the second quantum revolution, where outperforming classical metrology systems is a key goal.¹ This enhanced performance is characterized by an improvement in resolution, as well as improved sensitivity, that can approach the Heisenberg uncertainty limit, which scales as $1/N$ instead of $1/\sqrt{N}$ for classical sensors, where N is the number of photons. Within the field of quantum metrology, two main resources are pursued: continuous variables squeezed states and discrete photon number N00N states.¹ While the potential of quantum metrology using these resources is known,² a major challenge that needs to be addressed for wide usage of these systems is the low photon flux that is eventually used for detection. In quantum metrology systems, maintaining a low photon number is crucial. For example, some atomic systems can be depolarized due to the probe photon flux.³ In addition, biological samples can also be sensitive to the probe brightness, destructing or altering biological systems behavior.^{4,5} However, low brightness sources and lossy systems deeply degrade quantum imaging and sensing applications due to the long acquisition times of the measuring devices.⁵ Conversely, it is equally essential to achieve

high resolution in real time, which requires high-flux photon sources and efficient setups. Hence, the goal is to achieve the maximal photon flux possible (that is dictated by the system efficiency and source) while considering sample damage limitations. However, complex setups usually have unavoidable losses that prevent high flux quantum light⁶ from fulfilling their full potential in addition to their large footprint.⁷

Recently, structured light⁸ has been increasingly used to achieve better sensitivity in classical and quantum sensing schemes owing to its high dimensional nature, among them is optical rotation sensing. Optical rotation metrology is used for inertial navigation systems or for monitoring rotation in cryogenic environments⁹ among other applications. Structured light envisioned^{10,11} and enabled rotation sensing using twisted N00N states,⁷ polarization photonic gears,¹² and squeezed light.^{13,14} However, these studies faced challenges due to either inherent lossy systems that impeded the full potential of quantum light, lacked the measurement of mechanical rotation, or were degraded while increasing the dimensions of structured light. Therefore, the combination of structured and quantum light still faces major challenges due to complex and lossy systems, hindering true quantum advantage. A detailed comparison between

different quantum sensing schemes using structured light is given in the [supplementary material](#).

In our study, we sense rotations utilizing a new concept that we name **wavefront photonic gears** and quantum light. As the quantum light source we use robust and high brightness source for directly generating NOON states with $N = 2$.⁶ Our demonstration manages to address all the above-mentioned issues of combining quantum structured light: The rotation sensing mechanism uses very few elements with relatively low loss even for high-dimensional structured light, and its seamless integration is especially appealing for quantum light, which often poses significant challenges due to its low light levels. In addition, we address the dynamic challenges of real mechanical movements, allowing full 360° range of motion. These improvements are demonstrated through direct measurements of mechanical rotations and angular acceleration, maintaining coincidence count and visibility, thereby highlighting the real-world utility of our approach.

Using two spiral phase plates with opposite orientation, i.e., with topological charge of ℓ and $-\ell$, respectively, we convert mechanical rotations of a motor to wavefront phase shifts, hence allowing us to use interference to sense rotations, with ℓ -fold improvement in the angular resolution. Spiral phase plates are typically aligned so that the beam passes through the center of the plate, e.g., to convert a Gaussian beam to a Laguerre–Gaussian

beam.¹⁵ However, the region near the singularity of the plate may distort the beam and scatter part of it, owing to fabrication limitations. For the rotation sensing application that we present here, we overcome this limitation by sending the beam at some distance from the center of the spiral phase plate. By employing the NOON state source and coincidence detection in this system, we obtain an additional N -fold improvement in resolution. Hence, as will be shown in the following, the angular resolution scales as $N \times \ell$ and the sensitivity increases with ℓ .

In addition to super-resolved rotation sensing, our high brightness source combined with wavefront photonic gears allows us to measure fast rotations (reaching 10 deg/s) and angular acceleration (here measured at 1 deg/s²), which is a significant challenge in other, low efficiency schemes. With further reductions of both losses, as well as drift and improvements in detection efficiency, this scheme may enable us to approach unconditional violation of the shot noise limit for all the detected photons in the system.^{16,17}

II. THEORETICAL MODEL

Let us analyze the performance of the setup shown in [Fig. 1](#). Upon impinging a spiral phase plate (SPP), the Gaussian beam (Ψ_0) acquires a phase ϕ_1 ([Fig. 1](#)),

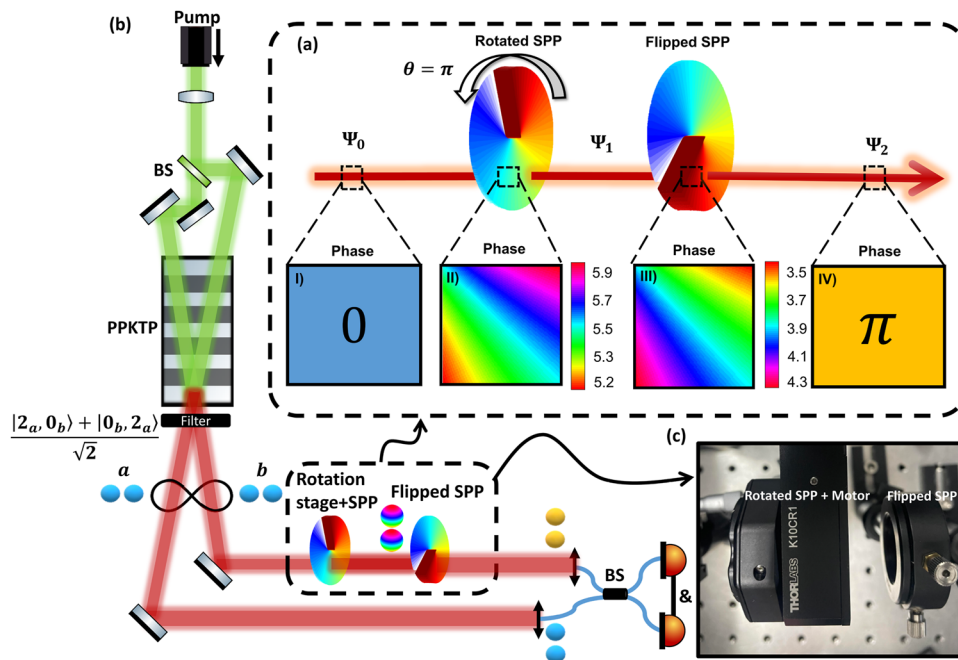


FIG. 1. Conceptual illustration of wavefront photonic gears and experimental setup. (a) A collimated Gaussian mode with a constant phase (I) passes through a spiral phase plate with topological number $\ell = 1$, accumulating a phase distribution (II). After a short propagation distance, the beam passes through a shifted reciprocal phase distribution (III), hence increasing the overall constant phase to π in this example (IV). (b) Experimental setup. Pump shaping enables the generation of a two-photon path entangled NOON state immediately after the nonlinear crystal. Next, the setup includes an MZI with two oppositely oriented SPPs, one of which is mounted on a rotation stage. After interfering at the beam splitter (BS), coincidence detectors record data for measuring coincidence count. The blue particles represent photons with no wavefront phase shift; the multi-colored particles represent structured photons, after the first SPP; and the yellow particles represent an example of π -shifted wavefront photons for the $\ell = 1$ case. (c) Experimental figure of the wavefront photonic gears apparatus. The first SPP is mounted on a rotation motor and the second, flipped, SPP is mounted without a motor. An alignment procedure for the apparatus appears in the [supplementary material](#).

$$\phi_1(x, y) = \begin{cases} \arctan\left(\frac{y}{x}\right)\ell, & x, y \in \Psi_0, \\ 0, & \text{otherwise.} \end{cases} \quad (1)$$

After impinging the second flipped SPP, the beam acquires the following phase ϕ_2 :

$$\phi_2(x, y) = \begin{cases} -\arctan\left(\frac{y}{x}\right)\ell + \theta\ell, & x, y \in \Psi_1, \\ 0, & \text{otherwise} \end{cases} \quad (2)$$

where Ψ_1 is a Gaussian beam with phase ϕ_1 that is displaced from the second SPP singularity. θ is the rotation angle that we wish to measure, and ℓ is the SPP topological charge. Hence, after two SPPs, the output beam Ψ_2 satisfies, classically,

$$\text{phase}(\Psi_2(x)) = \text{phase}(\Psi_0(x)) + \theta\ell. \quad (3)$$

Namely, at a given setting of the spiral phase plates, the output beam acquires a constant $\theta\ell$ phase. Therefore, the two SPPs serve as a wavefront photonic gear, converting mechanical rotation to flat phase delay, which is dependent on the topological charge of the SPP. We assume that the second SPP is in the near field of Ψ_1 . Our scheme differs from other photonic gears implementations^{12,18} by eliminating the need for polarization handling. This feature enhances its versatility, enabling to improve the sensitivity in various interferometric configurations.

We now turn to analyze how wavefront photonic gears can be enhanced by quantum entanglement, here analyzed for the case of

N00N states with $N = 2$ that will be denoted 2002. According to Eq.(3), a single arm of a Mach-Zehnder interferometer (MZI) accumulates a phase of $\theta\ell$. Hence, after rotation of a single SPP in a single arm of the path entangled 2002 state, the state accumulates $2\theta\ell$ according to

$$|\psi\rangle = |2a, 0_b\rangle + e^{i2\theta\ell}|0_a, 2_b\rangle, \quad (4)$$

where a and b denote the two arms of the interferometer. By mixing the output of the two arms using a 50:50 beam splitter, the final state before the detectors is⁶

$$|\psi\rangle_{2002} = \sin(\theta\ell)\frac{|2\rangle|0\rangle + |0\rangle|2\rangle}{\sqrt{2}} + \cos(\theta\ell)|1\rangle|1\rangle. \quad (5)$$

Hence, by rotating one of the SPPs and measuring the coincidence (i.e., the $|1\rangle|1\rangle$ state), the signal oscillates $N \times \ell$ times for 360° rotation (in our specific case $2 \times \ell$), thus exhibiting super-resolution. This occurs because the probability of detection equals to $\cos^2(\theta\ell) = \frac{1+\cos(2\theta\ell)}{2}$, resulting in a detection peak every $2\theta\ell = 2 \times q \times \pi$ radians where q is an integer.

Following Refs. 7 and 11, this sets the following bound on the uncertainty (Heisenberg limit):

$$\Delta\theta = \frac{\langle\Delta\hat{M}\rangle}{\left|\frac{\partial\langle\hat{M}\rangle}{\partial\theta}\right|} = \frac{1}{\sqrt{MN\ell}}, \quad (6)$$

where \hat{M} is the measurement operator $\hat{M} = \sum_{i=1}^M |\psi\rangle_i \langle\psi|_i$, representing M independent N -photon N00N states, which saturates the

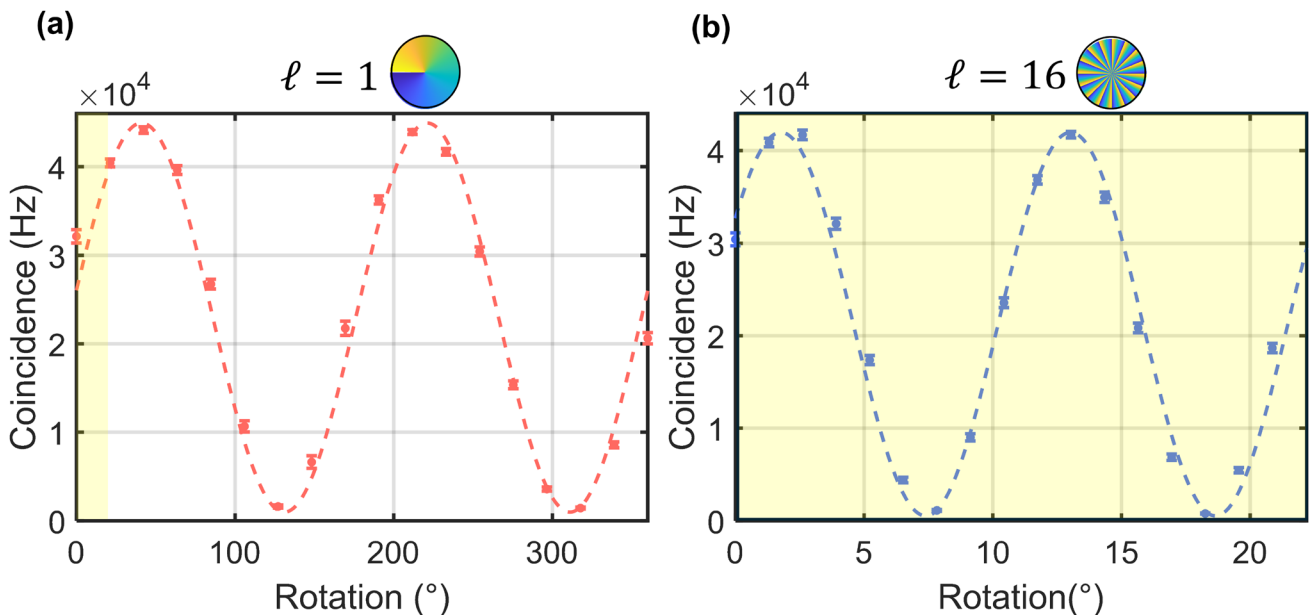


FIG. 2. Coincidence counts vs rotation angle plots for $\ell = 1$ and $\ell = 16$. Both the figures demonstrate that the detected signals exhibit super resolution. In the case of $\ell = 16$, the coincidence count oscillates 16 times more over a 360° rotation than in the $\ell = 1$ scenario (and both oscillate twice times more than the classical case). Each data point comprises 20 measurements taken from 20 different rotation experiments; all aligned using cross-correlation analysis. The shaded yellow area corresponds to the segment where the signal with $\ell = 16$ performs two oscillations, for comparison.

quantum Cramer–Rao bound.⁴ Hence, it is of interest to use quantum entanglement and push the sensitivity further using the $1/N$ scaling, whereas the shot noise limited error scales as $1/\sqrt{N}$. Importantly, in our work, we benefit from all three multiplicative in the denominator in Eq. (6) in a manner that pushes the sensitivity in real-life scenarios. We use $N = 2$ using a bright N00N state source, hence increasing M . In addition, we increase the topological charge number and avoid aperture limitations, resulting in a negligible coincidence pair loss (the coincidence rate dropped by 4.8% percent, from 44.9 k/s with $\ell = 1$ to 42.7 k/s with $\ell = 16$, as shown in Fig. 2). The observed change could be smaller as we bring the SPP plates closer together. This is supported by simulations provided in the [supplementary material](#), which showcase the potential of wavefront photonic gears with a minimal trade-off between higher topological charges and coincidence counts compared to other methods. These simulations estimate the beam modal change when passing through wavefront photonic gears and the expected influence of higher topological charge numbers on that change (see Table S2 in the [supplementary material](#)).

III. EXPERIMENTAL SETUP

The experimental setup is shown in Fig. 1. The quantum source is a bright N00N state source that consists of a continuous wave 532.25 nm laser with output power of 75 mW after the residual pump filter, a beam splitter, and a 2 cm PPKTP crystal poled for type-0 interaction⁶ held inside an oven with a temperature of 36 °C. It is followed by a Mach–Zehnder interferometer that utilizes the wavefront photonic gears mechanism, consisting of two opposite SPPs, where the first one is mounted on a mechanical rotation stage.

The two SPPs are positioned such that the beam passes roughly 2 mm from the singularity point at the center of the SPPs. The two SPPs are located 5 cm from one another. The two N00N state paths are then coupled to two 1064 nm single mode polarization maintaining fiber and interfere inside a 50:50 fiber beam splitter. Then, photons from the two arms are detected using two (SNSPDs) superconducting nanowire single photon detectors (Single Quantum Eos) with 81% and 86% efficiency.

IV. ROTATION MEASUREMENT

We measured the coincidence at different angles for $\ell = 1$ and $\ell = 16$, that were attached to a mechanical motor and were equally spaced. We analyzed the data using a weighted least squares fit, where each point was weighted by the reciprocal of the measured variance, from a set of 20 repeated measurements⁷ (that allows us to capture the inherent noise of the system). The resulting fitted curve is as follows:⁷

$$\frac{A}{2} \left[1 - \cos \left(\frac{\pi N \ell}{180^\circ} \theta - C \right) \right] + B, \quad (7)$$

where A is the amplitude of the cosine curve, B is the offset, and C is the parameter specifying the initial rotation point. Thus, the expression $\left[\frac{A}{A+2B} \right]$ provides an estimation of the curve's visibility, as determined by the fit. Mechanical rotation displacement causes increased drift in the detected signal. Therefore, each of the 20 measurements commenced from a distinct relative phase between the two arms. To tackle this issue, we employed a cross-correlation analysis to identify the relative phase (“ C ”) of each measurement. Then, we aligned each measurement correctly with the desired starting

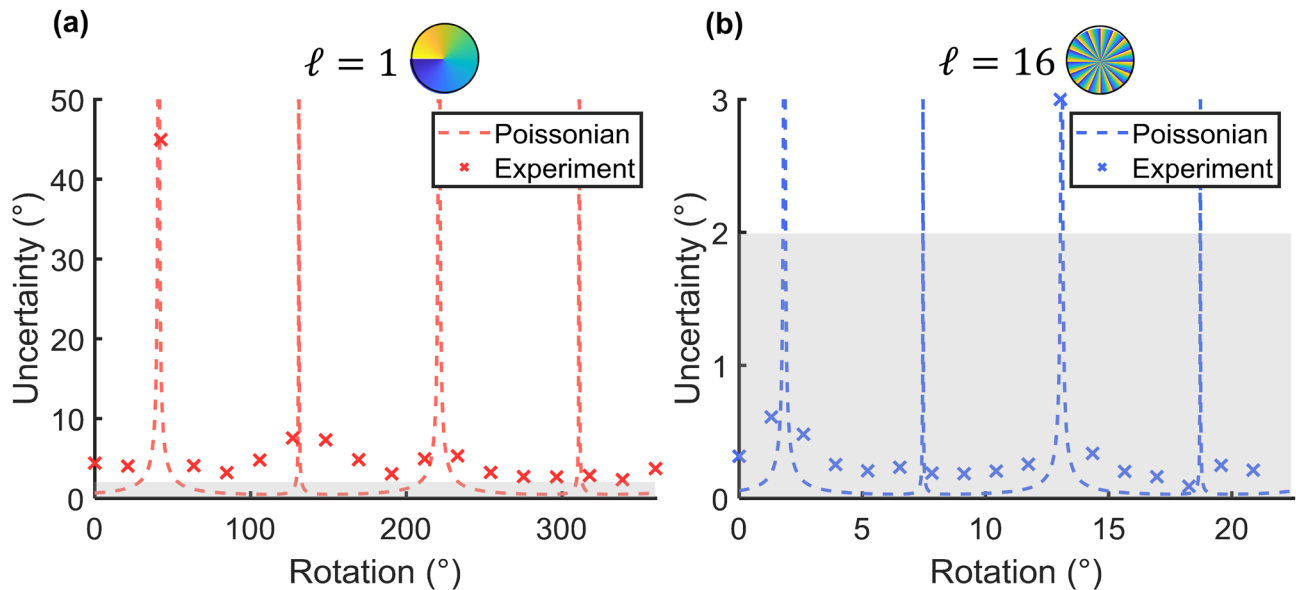


FIG. 3. Angular uncertainty for two cases: $\ell = 1$ in red and $\ell = 16$ in blue. The dashed curves are calculated from Eq. (8) while taking into account Poissonian errors for $\Delta M(\theta)$, as determined from Eq. (7). The crosses represent experimentally determined precision values calculated using Eq. (8), where for this case, $\Delta M(\theta)$ signifies the standard deviation of a single rotation measurement. The shaded area corresponds to the same uncertainty values, for comparison.

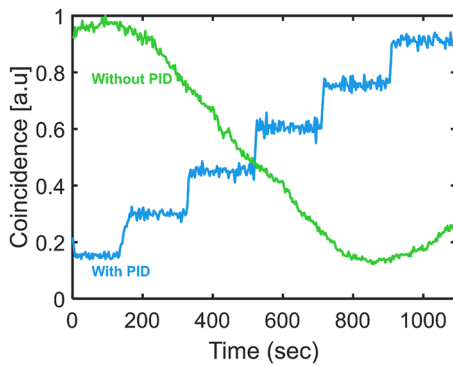


FIG. 4. Interferometer stabilization with photonic gears. The blue curve demonstrates stable coincidence counts due to the use of a PID controller. The controller successfully stabilized the interferometer on different phase (coincidence) values. The green curve shows unstable coincidence counts, illustrating the ongoing drift of the interferometer without stabilization.

point on the curve. (See the [supplementary material](#) for details on the cross-correlation analysis.)

Figure 2 shows the results of two experiments, one with $\ell = 1$ and the other with $\ell = 16$ with an acquisition time of 0.1 s and a coincidence window of 0.5 ns, normalized to coincidence per second. Clearly, the coincidence count exhibits super resolution due to quantum correlations, where in $\ell = 1$, the detected pairs oscillate twice in a 360° rotation and in $\ell = 16$, the coincidence count oscillate 32 times (here, we show almost two oscillations in 20.8°). For each of these measurements, the visibility values are (95.7%) and (97.6%) respectively.

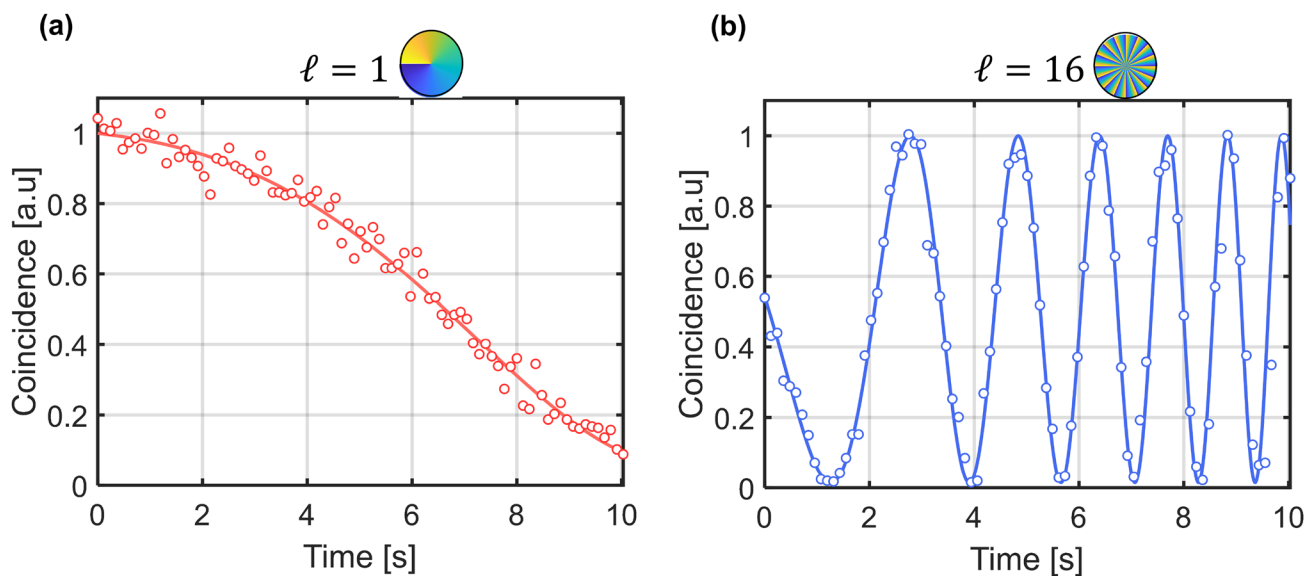


FIG. 5. Acceleration measurements. Experimental (circles) and least square fitting function (continuous curves) for a rotating motor under constant acceleration (1 deg/s^2) over a 10-s duration. Two distinct topological charges, $\ell = 1$ and $\ell = 16$, were employed. Acceleration measurements were extracted from the fitted curves.

We compute the angular uncertainty using the following equation:⁷

$$\Delta\theta = \frac{\Delta M(\theta)}{\frac{AN\ell\pi}{360^\circ} \left| \sin\left(\frac{\pi N\ell}{180^\circ}(\theta - C)\right) \right|}, \quad (8)$$

where $\Delta M(\theta)$ represents the standard deviation for each measurement angle, calculated from 20 measurements. The angular precision results are shown in Fig. 3 for $\ell = 1$ and $\ell = 16$. The lowest uncertainty for $\ell = 1$ ($\ell = 16$) is 2.28° (0.09°) degrees. At the oscillation peaks, where the cosine derivative is zero, the rotation angle becomes unmeasurable, leading to increased uncertainty, as shown in Fig. 3.

Importantly, by utilizing larger values of ℓ , we obtained a 25-fold experimental uncertainty reduction associated with $\ell = 16$ compared to our baseline measurements at $\ell = 1$, without changing the acquisition time and the number of coincidence counts. This aligns with our simulations presented in the [supplementary material](#). Compared to the regular method of passing through the center, avoiding the manufacturing defects improve the visibility and coincidence count significantly for $\ell = 1$. For $\ell = 16$, passing through the center decreases the signal to zero (see the [supplementary material](#)).

Increasing ℓ allows us to approach the Poissonian error regime, which coincides with the shot noise limit, as shown in Fig. 3. In particular, for $\ell = 1$, the minimal uncertainty is 4.5 higher than the Poissonian errors regime. Conversely, for $\ell = 16$, our measurements are 2.2 higher than the Poissonian errors regime, which is attributed to the decreased mechanical rotation for detecting a single oscillation. The gap between the expected and desired results is primarily due to discrepancies arising from changes in coupling due to mechanical rotation, and interferometer drift during extended measurements using a physical motor. This gap can be mitigated using

a specially built mechanical rotor that will have less effect on the stability of the interferometer and active interferometer stabilizers.

In the analysis above, we considered only the coincidentally detected photons, but the single count rate for both detectors are roughly 500 000 and 490 000, compared to 45 000 coincidence detections per second. To reach unconditional violation of the shot noise limit with two photon N00N states, the system efficiency and visibility must satisfy $\eta^N V^2 N > 1$, where η is the Klyshko efficiency (here measured as 9%) and V is the visibility.¹⁷ Assuming near unity detection efficiency,¹⁹ we need to increase the coupling efficiency, which constitutes the main loss mechanism, by a factor of 7 from 10% to 71% (for example, using objective lenses and alignment stages with tilt and rotation). We note that even though unconditional violation of the shot noise limit was not achieved, a quantum enhancement (super resolution) is clearly present and helps accurately measure angular acceleration, as shown in the following. In addition, having the phase shift in the signal and idler wavelengths is beneficial due to material dispersion,¹⁷ challenging fabrication in shorter wavelengths, and limited transparency in the ultra violet for fused silica.

V. INTERFEROMETER STABILIZER

Photonic gears demonstrate multiple functionalities, including use as an interferometer stabilizer. To test this, we employed a PID controller to stabilize the interferometer at different phases. In the first measurement, the motor maintained the interferometer at various phases (constant coincidence counts) for 200 s each before moving to the next phase, using a PID feedback loop from a time tagger. In a subsequent measurement, we did not rotate the motor, allowing us to observe the drift in coincidence counts without stabilization. The blue curve (“With PID”) in Fig. 4 shows stable coincidence counts at different angles due to the PID controller, while the green curve (“Without PID”) shows unstable coincidence counts, highlighting the ongoing drift without stabilization.

VI. ACCELERATION MEASUREMENT

Notably, using our high-brightness scheme and wavefront photonic gears, we are not limited to slowly varying angular displacement but can measure fast rotations and angular acceleration, using structured quantum light. Here, we measured the acceleration of a rotating motor using an acquisition time of 0.01 s. The motor was subjected to a constant acceleration of 1 deg/s² and the measurement was limited to T = 10 s. The measurements were executed using our wavefront photonic gear sensor, employing two distinct topological charges, $\ell = 1$ and $\ell = 16$. To estimate the given rotation, we fitted a chirp function to the detected coincidence pair count (Fig. 5),

$$\frac{A}{2} \left[1 - \cos \left(\theta_0 + \frac{\pi N \ell}{180} \omega_0 t + \frac{k}{2} t^2 \right) \right] + B, \tag{9}$$

where $k = \frac{\pi N \ell (\omega_f - \omega_0)}{180 T}$ is the acceleration parameter that we wish to measure, from which the angular acceleration can be extracted. Here, $\frac{\pi N \ell}{180} \omega_0$ (ω_f) is the initial (final) angular frequency and θ_0 is the initial phase. Using least squares fit for $\ell = 1$, we registered an acceleration of 1.51 deg/s² squared, which is quite far from the

nominal angular acceleration of 1 deg/s² squared. However, for $\ell = 16$, we obtained a measurement of $1.015^\circ \pm 0.021^\circ$ deg/s². For $\ell = 1$, the 10 s measurement duration proved inadequate for achieving a precise fit. This limitation arises due to the numerous potential fitting functions applicable in such circumstances. Therefore, the enhanced super-resolution provided by higher ℓ values and photon numbers N contributes to shorter measurement time and improved accuracy.

VII. CONCLUSIONS

We demonstrated a new rotation sensing mechanism that uses quantum light and just two spiral phase plates. The small footprint of wavefront photonic gears makes it highly suitable for real-life scenarios. This scheme does not need any additional beam manipulation with respect to other MZI: the two phase plates are on-axis and merely put inside an already established MZI scheme. Remarkably, there is no decrease in visibility and only a negligible reduction in the detected pair rate is measured when using different topological charges of the SPPs. Hence, we envision that the concept of wavefront photonic gears can be used with much higher topological charge SPPs or even spiral phase mirrors²⁰ without major complications, such as degrading beam quality. The reason is that usually, SPPs are manufactured with an unavoidable singularity point that is usually neglected for large beams. Moreover, high spatial frequencies near the SPP’s singularity contribute to diffraction at sharper angles. However, our system successfully eliminates these constraints, operating in close proximity to the singularity. The two phase plates can be positioned adjacent to each other, which reduces footprint and may mitigate the diffraction effects of higher topological charges. Interestingly, while we do not use SPPs in a conventional manner, the quantum light complexity and, therefore, its structure²¹ changes between the two SPPs. This allows us to have a metrological equivalence to other quantum structured light schemes, which are based on free space modes. The high brightness of our source, together with the system efficiency, allowed us to use it for measuring angular acceleration and fast angular rotations that may help measure the rotation angle at any given angle using real-time feedback control.²² In addition to the demonstration of mechanical rotation sensing, our demonstration also improved the bright N00N state source visibility⁶ to near unity. This marks our scheme as a prime candidate for multi-photon sensing schemes along with structured light, increasing the resolution using higher order photon pairs events. The concept of wavefront photonic gears is not limited to quantum light and can be also used with classical light, by simply using two phase plates and conventional interferometers. In addition, the sensitivity may be increased by repeatedly passing through various locations on the same SPP, mimicking the advantages of multi-pass sensing schemes.²³ Finally, one can generalize our scheme to sense linear displacement in the same manner¹⁸ or to combine squeezed light with wavefront photonic gears.²⁴

SUPPLEMENTARY MATERIAL

Additional data tables, extended experimental details, and supplementary figures are available in the [supplementary material](#).

This [supplementary material](#) provides in-depth information supporting the findings of this study.

ACKNOWLEDGMENTS

We acknowledge the support from the Tel Aviv University Center for Quantum Science and Technology, the Israel Science Foundation (Grant No. 969/22), and the PAZY Foundation.

AUTHOR DECLARATIONS

Conflict of Interest

The authors have no conflicts to disclose.

Author Contributions

O.Y. and G.T. contributed equally to this work.

Ofir Yesharim: Conceptualization (lead); Data curation (equal); Formal analysis (equal); Investigation (equal); Methodology (equal); Software (equal); Validation (equal); Visualization (equal); Writing – original draft (equal); Writing – review & editing (equal). **Guy Tshuva:** Conceptualization (supporting); Data curation (equal); Formal analysis (equal); Investigation (equal); Methodology (equal); Software (equal); Validation (equal); Visualization (equal); Writing – original draft (equal); Writing – review & editing (equal). **Ady Arie:** Conceptualization (supporting); Funding acquisition (equal); Project administration (equal); Resources (equal); Supervision (equal); Writing – review & editing (equal).

DATA AVAILABILITY

The data that support the findings of this study are available from the corresponding authors upon reasonable request.

REFERENCES

- 1 E. Polino, M. Valeri, N. Spagnolo, and F. Sciarrino, “Photonic quantum metrology,” *AVS Quantum Sci.* **2**, 024703 (2020).
- 2 H. Grote, K. Danzmann, K. L. Dooley, R. Schnabel, J. Slutsky, and H. Vahlbruch, “First long-term application of squeezed states of light in a gravitational-wave observatory,” *Phys. Rev. Lett.* **110**, 181101 (2013).
- 3 F. Wolfgramm, C. Vitelli, F. A. Beduini, N. Godbout, and M. W. Mitchell, “Entanglement-enhanced probing of a delicate material system,” *Nat. Photonics* **7**, 28–32 (2013).
- 4 M. A. Taylor and W. P. Bowen, “Quantum metrology and its application in biology,” *Phys. Rep.* **615**, 1–59 (2016).
- 5 Z. He, Y. Zhang, X. Tong, L. Li, and L. V. Wang, “Quantum microscopy of cells at the Heisenberg limit,” *Nat. Commun.* **14**, 2441 (2023).
- 6 G. Di Domenico, S. Pearl, A. Karnieli, S. Trajtenberg-Mills, I. Juwiler, H. S. Eisenberg, and A. Arie, “Direct generation of high brightness path entangled N00N states using structured crystals and shaped pump beams,” *Opt. Express* **30**, 21535–21543 (2022).
- 7 M. Hiekkamäki, F. Bouchard, and R. Fickler, “Photonic angular superresolution using twisted N00N states,” *Phys. Rev. Lett.* **127**, 263601 (2021).
- 8 A. Forbes, M. de Oliveira, and M. R. Dennis, “Structured light,” *Nat. Photonics* **15**, 253–262 (2021).
- 9 P. Chen, B. J. Albert, C. Gao, N. Alaniva, L. E. Price, F. J. Scott, E. P. Saliba, E. L. Sesti, P. T. Judge, E. W. Fisher, and A. B. Barnes, “Magic angle spinning spheres,” *Sci. Adv.* **4**, eaau1540 (2018).
- 10 Y. Ming, J. Tang, Z.-x. Chen, F. Xu, L.-j. Zhang, and Y.-q. Lu, “Generation of N00N state with orbital angular momentum in a twisted nonlinear photonic crystal,” *IEEE J. Sel. Top. Quantum Electron.* **21**, 225–230 (2015).
- 11 A. K. Jha, G. S. Agarwal, and R. W. Boyd, “Supersensitive measurement of angular displacements using entangled photons,” *Phys. Rev. A* **83**, 053829 (2011).
- 12 V. D’Ambrosio, N. Spagnolo, L. Del Re, S. Slussarenko, Y. Li, L. C. Kwek, L. Marrucci, S. P. Walborn, L. Aolita, and F. Sciarrino, “Photonic polarization gears for ultra-sensitive angular measurements,” *Nat. Commun.* **4**, 2432 (2013).
- 13 K. Liu, C. Cai, J. Li, L. Ma, H. Sun, and J. Gao, “Squeezing-enhanced rotating-angle measurement beyond the quantum limit,” *Appl. Phys. Lett.* **113**, 261103 (2018).
- 14 Z. Li, H. Guo, H. Liu, J. Li, H. Sun, R. Yang, K. Liu, and J. Gao, “Higher-order spatially squeezed beam for enhanced spatial measurements,” *Adv. Quantum Technol.* **5**, 2200055 (2022).
- 15 S. S. R. Oemrawsingh, J. A. W. van Houwelingen, E. R. Eliel, J. P. Woerdman, E. J. K. Verstegen, J. G. Kloosterboer, and G. W. ’t Hooft, “Production and characterization of spiral phase plates for optical wavelengths,” *Appl. Opt.* **43**, 688–694 (2004).
- 16 K. J. Resch, K. L. Pregnell, R. Prevedel, A. Gilchrist, G. J. Pryde, J. L. O’Brien, and A. G. White, “Time-reversal and super-resolving phase measurements,” *Phys. Rev. Lett.* **98**, 223601 (2007).
- 17 S. Slussarenko, M. M. Weston, H. M. Chrzanowski, L. K. Shalm, V. B. Verma, S. W. Nam, and G. J. Pryde, “Unconditional violation of the shot-noise limit in photonic quantum metrology,” *Nat. Photonics* **11**, 700–703 (2017).
- 18 R. Barboza, A. Babazadeh, L. Marrucci, F. Cardano, C. de Lisio, and V. D’Ambrosio, “Ultra-sensitive measurement of transverse displacements with linear photonic gears,” *Nat. Commun.* **13**, 1080 (2022).
- 19 D. V. Reddy, R. R. Nerem, S. W. Nam, R. P. Mirin, and V. B. Verma, “Superconducting nanowire single-photon detectors with 98% system detection efficiency at 1550 nm,” *Optica* **7**, 1649–1653 (2020).
- 20 R. Fickler, G. Campbell, B. Buchler, P. K. Lam, and A. Zeilinger, “Quantum entanglement of angular momentum states with quantum numbers up to 10,010,” *Proc. Natl. Acad. Sci. U. S. A.* **113**, 13642–13647 (2016).
- 21 I. Nape, B. Sephton, P. Ornelas, C. Moodley, and A. Forbes, “Quantum structured light in high dimensions,” *APL Photonics* **8**, 051101 (2023).
- 22 A. A. Berni, T. Gehring, B. M. Nielsen, V. Händchen, M. G. A. Paris, and U. L. Andersen, “*Ab initio* quantum-enhanced optical phase estimation using real-time feedback control,” *Nat. Photonics* **9**, 577–581 (2015).
- 23 Y. Israel, J. L. Reynolds, B. B. Klopfer, and M. A. Kasevich, “Continuous wave multi-pass imaging flow cytometry,” *Optica* **10**, 491–496 (2023).
- 24 J. Qin, Y.-H. Deng, H.-S. Zhong, L.-C. Peng, H. Su, Y.-H. Luo, J.-M. Xu, D. Wu, S.-Q. Gong, H.-L. Liu, H. Wang, M.-C. Chen, L. Li, N.-L. Liu, C.-Y. Lu, and J.-W. Pan, “Unconditional and robust quantum metrological advantage beyond N00N states,” *Phys. Rev. Lett.* **130**, 070801 (2023).